Published in final edited form as:

Acta Biomater. 2018 April 01; 70: 154–164. doi:10.1016/j.actbio.2018.01.050.

Towards the Scale up of Tissue Engineered Intervertebral Discs for Clinical Application

Sarah E. Gullbrand[1,2], **Dong Hwa Kim**[1,2], **Edward Bonnevie**[1,2], **Beth G. Ashinsky**[1,2], **Lachlan J. Smith**[1,2,3], **Dawn M. Elliott**[4], **Robert L. Mauck**[1,2], **Harvey E. Smith**[1,2]

[1]Translational Musculoskeletal Research Center, Corporal Michael J. Crescenz VA Medical Center, Philadelphia, PA

[2]McKay Orthopaedic Research Laboratory, Department of Orthopaedic Surgery, University of Pennsylvania, Philadelphia, PA

[3]Department of Neurosurgery, University of Pennsylvania, Philadelphia, PA

[4]Department of Biomedical Engineering, University of Delaware, Newark, DE

Abstract

Replacement of the intervertebral disc with a viable, tissue-engineered construct that mimics native tissue structure and function is an attractive alternative to fusion or mechanical arthroplasty for the treatment of disc pathology. While a number of engineered discs have been developed, the average size of these constructs remains a fraction of the size of human intervertebral discs. In this study, we fabricated medium (3 mm height x 10 mm diameter) and large (6 mm height x 20 mm diameter) sized disc-like angle ply structures (DAPS), encompassing size scales from the rabbit lumbar spine to the human cervical spine. Maturation of these engineered discs was evaluated over 15 weeks in culture by quantifying cell viability and metabolic activity, construct biochemical content, MRI T2 values, and mechanical properties. To assess the performance of the DAPS in the *in vivo* space, pre-cultured DAPS were implanted subcutaneously in athymic rats for 5 weeks. Our findings show that both sized DAPS matured functionally and compositionally during *in vitro* culture, as evidenced by increases in mechanical properties and biochemical content over time, yet large DAPS under-performed compared to medium DAPS. Subcutaneous implantation resulted in reductions in NP cell viability and GAG content at both size scales, with little effect on AF biochemistry or metabolic activity. These findings demonstrate that engineered discs at large size scales will mature during *in vitro* culture, however, future work will need to address the challenges of reduced cell viability and heterogeneous matrix distribution throughout the construct.

Keywords

tissue engineering; hydrogel; electrospun scaffold; subcutaneous implantation; scale up; translation; animal model

*Corresponding Author: Harvey E. Smith, MD, Department of Orthopaedic Surgery, University of Pennsylvania, 3737 Market Street, 6th Floor, Philadelphia, PA 19104, Harvey.Smith@uphs.upenn.edu, 800-789-7366.

Disclosures

The authors declare no potential conflicts of interest with respect to the research, authorship and/or publication of this manuscript.

1. Introduction

The intervertebral discs (IVD) of the spine are fibrocartilaginous composite structures comprised of an inner nucleus pulposus (NP) composed primarily of proteoglycans, type II collagen and water, and an outer annulus fibrosus (AF) composed of aligned types I and II collagen organized into concentric lamellae [1]. When healthy IVDs are loaded, hydrostatic pressure develops in the NP, placing the AF in tension and allowing the tissue to bear load while permitting motion [2]. This structure-function relationship is disrupted with degeneration of the IVD, a complex and multifactorial cascade of biochemical, cellular and structural changes that is commonly associated with low back pain [3,4].

Low back pain is a top three cause of disability in developed nations, and in the United States is associated with a yearly economic burden of approximately $200 billion due to medical costs and lost wages [5,6]. For patients with end-stage IVD degeneration who are unresponsive to conservative treatment, the gold standard surgical treatment is fusion to immobilize the affected motion segment. Fusion does not restore native IVD structure or function, is associated with degeneration of adjacent segments, and randomized controlled trials show similar clinical outcomes compared to non-operative treatment [7,8]. Artificial total disc arthroplasty devices are also utilized as an alternative to fusion, in an effort to preserve spinal motion and prevent degeneration of adjacent segments [9]. The use of mechanical arthroplasty in the lumbar spine for treatment of back pain is somewhat controversial, with some evidence that current lumbar artificial total disc arthroplasty devices offer no significant clinical benefit over fusion [10]. There is greater enthusiasm for cervical mechanical disc arthroplasty, but uncertainty regarding potential for mechanical wear debris and the long-term revision options limits application. Thus, there is a significant need to develop new treatment strategies for patients with IVD degeneration and associated axial spine pain and neurogenic extremity pain.

Tissue engineering offers considerable promise for the treatment of end stage disease, as replacement of the degenerative IVD with a viable engineered construct may restore healthy spine function with the capacity to remodel in response to the *in vivo* environment. Towards this end, composite IVDs with tissue-engineered NP and AF analogs have been developed by several groups and evaluated *in vitro* and *in vivo* in small and large animal models [11-18]. Our group in particular has developed tissue-engineered disc-like angle ply structures (DAPS), composed of engineered NP and AF analogs. The AF region is comprised of cell-seeded concentric layers of electrospun, nanofibrous poly (ε-caprolactone) (PCL), with alternating fiber alignments of ±30°, to recapitulate the native hierarchical structure of the AF. The PCL AF is combined with a hyaluronic acid or agarose hydrogel that serves as the NP region to form a complete composite tissue-engineered IVD [19]. We have previously fabricated DAPS sized for the rabbit lumbar spine and rat caudal disc space, and shown compositional equivalence of the DAPS with native tissue with extended *in vitro* culture times [19,20] and stability upon *in vivo* implantation [21].

Despite the progress over the past decade in the field of IVD tissue engineering, engineered constructs have thus far only been fabricated at length scales that are a fraction of the size of human IVDs. The average width and height of engineered IVDs reported in the literature are

approximately 11 mm and 3 mm, respectively, while human cervical IVDs are an average 30 mm in lateral width and 6 mm in height, and human lumbar IVDs are an average 55 mm in lateral width and 11 mm in height [22-24]. Fabrication of tissue-engineered IVDs at larger size scales is therefore a critical next step towards the clinical translation of this technology. The purpose of this study was therefore to fabricate and culture DAPS at multiple length scales, the largest of which mimics the scale of a human cervical IVD. At each length scale, we evaluated construct viability, matrix distribution and mechanical properties over 15 weeks culture *in vitro*, as well as after a 5 week period of *in vivo* subcutaneous implantation.

2. Methods

2.1 Disc Cell Isolation and DAPS Fabrication

NP and AF tissues were isolated from three adult bovine caudal spines, purchased from a local abattoir with institutional approval, and incubated overnight at 37°C in high glucose Dulbecco's modified Eagle's medium (DMEM) containing 2% penicillin/streptomycin/fungizone (PSF, Antibiotic-Antimycotic; Gibco) and 10% fetal bovine serum (FBS). Tissues were then digested, first in 2.5 mg/mL pronase for 1 hour, followed by 0.5 mg/mL collagenase (Type IV, Sigma-Aldrich, St. Louis, MO) for 4 hours (NP tissue) or 8 hours (AF tissue). Cells were then filtered through a 70 μm strainer before plating onto tissue culture plastic in DMEM containing 1% PSF and 10% FBS (basal media). NP and AF cells were expanded to passage 2 prior to DAPS seeding.

DAPS were fabricated in two sizes – medium (10 mm diameter, 3 mm height), and large (20 mm diameter, 6 mm high). DAPS were cultured for the duration of the study in standard culture conditions (21% O_2, 5% CO_2, 37°C). To fabricate the NP region of the DAPS, NP cells were trypsinized, suspended in chemically defined media at a density of 40 x 10^6 cells/mL, and mixed with molten 4% w/v agarose (49°C, Type VII, Sigma-Aldrich). The agarose/cell solution (20 x 10^6 cells/mL, 2% agarose) was then cast into 6 well plates to generate agarose slabs of the desired height. These were then punched with sterile biopsy punches to create NP regions either 6 mm thick and 10 mm diameter (for large DAPS), or 3 mm thick and 5 mm diameter (for medium DAPS). NP hydrogels were cultured in isolation for 2 weeks on an orbital shaker (prior to combining with the AF region of the DAPS) in chemically defined medium (CM+) comprised of high glucose DMEM supplemented with 1% PSF, 40 ng/mL dexamethasone (Sigma-Aldrich), 50 μg/mL ascorbate 2-phosphate (Sigma-Aldrich), 40 μg/mL L-proline (Sigma-Aldrich), 100 μg/mL sodium pyruvate (Corning Life Sciences, Corning, NY), 0.1% insulin, transferrin, and selenious acid (ITS Premix Universal Culture Supplement; Corning), 1.25 mg/mL bovine serum albumin (Sigma-Aldrich), 5.35 μg/mL linoleic acid (Sigma-Aldrich), and 10 ng/mL TGF-β3 (R&D Systems, Minneapolis, MN). The media was changed three times per week. Each medium size NP hydrogel received 1.5 mL of media and each large size hydrogel received 7 mL of media.

To fabricate the AF region of the DAPS, a 14.3% w/v solution of poly(ε-caprolactone) (PCL) dissolved in a 1:1 mixture of tetrahydrofuran and N,N-dimethylformamide was electrospun onto a grounded, rotating mandrel to produce a sheet of aligned nanofibers, as previously described [25]. To replicate the native lamellar architecture of the rabbit and goat

IVDs for medium and large DAPS, electrospun sheets of PCL were fabricated at 250 μm and 350 μm thickness, respectively. Strips of electrospun PCL were cut at an angle of 30° to the fiber direction. Strips 3 mm thick and 150 mm in length were used to fabricate medium DAPS, while strips 6 mm thick and 210 mm in length were used to fabricate large DAPS. PCL strips were hydrated through a gradient of ethanol (100%, 70%, 50%, 30% and phosphate buffered saline), prior to coating overnight in a solution of 20 μg/mL fibronectin (Sigma-Aldrich) in phosphate buffered saline (PBS). AF cells were suspended in basal media and seeded onto the PCL strips at a density of 1.5×10^6 cells per side for medium DAPS and 4.2×10^6 cells per side for large DAPS. AF cell-seeded strips were cultured in CM+ for 1 week. To assemble the AF region of the DAPS, either two (for medium DAPS) or four (for large DAPS) strips were coupled to achieve opposing fiber directions (±30°), and then wrapped using a custom mold as previously described [19] to create a concentric, lamellar construct with an outer diameter of 10 mm for medium DAPS and 20 mm for large DAPS. The AF region of the DAPS was cultured alone in CM+ for one week on an orbital shaker, at which point the AF and NP regions of the DAPS were combined.

Combined DAPS were then cultured in CM+ media on an orbital shaker, with media changed three times per week. Medium DAPS received 5 mL of media per construct, and large DAPS received 20 mL of media per construct. At 5, 10 and 15 weeks total culture duration, DAPS of each size were collected for viability assays (n=3), magnetic resonance imaging (n=3), mechanical testing (n=3), biochemical assays (n=6), and histology (n=2-3), as detailed below.

2.2 Viability and Metabolic Activity

At each time point, three DAPS of each size were cut in half, with one-half utilized for assays of NP cell viability and AF metabolic activity. The remaining half was reserved for biochemical assays, as detailed in section 2.5. The AF and NP regions of the DAPS were manually separated. Cell viability in the hydrogel NP region was quantified using a Live/Dead cell viability kit (Molecular Probes, Invitrogen Life Technologies). 10X images from five fields of view (center, top, bottom, left, right) of each hydrogel were obtained using an inverted fluorescence microscope (Nikon Eclipse Ti-S), and the number of live and dead cells in each region were counted using a custom MATLAB code as previously described [26].

Metabolic activity of cells in the AF region of the DAPS was quantified via the MTT colorimetric assay. The AF region of the DAPS was immersed in a solution of DMEM and 0.5 mg/mL MTT and incubated for 5 hours at 37°C and 5% CO_2. The AF region was then finely minced, and the formazan product solubilized in dimethyl sulfoxide. Absorbance was measured on a microplate reader at 540 nm, and normalized to sample wet weight to correct for variations in construct size.

2.3 Mechanical Testing

To determine compressive mechanical properties over the culture duration, DAPS were subjected to mechanical testing in unconfined compression (Instron 5948, Norwood, MA) using a protocol previously used to quantify the mechanical properties of native disc tissue

[27,28]. A 0.05 N pre-load was applied, followed by 20 cycles of compressive loading at 0.5 Hz from 0.05 N to 18 N for medium DAPS, and 0.05 N to 75 N for large DAPS (0.24 MPa, comparable to the stress imposed by ~0.5 body weight to a human disc) [28]. The stress-strain response of each DAPS was analyzed using a bi-linear fit in MATLAB to quantify the toe and linear region moduli, transition strain, and compressive range of motion (ROM).

2.4 Compositional Evaluation

To evaluate DAPS collagen and glycosaminoglycan (GAG) content, the AF and NP regions of the DAPS were separated and individually digested overnight in proteinase K at 60°C. DNA content of each sample was quantified via the Quanti-iT PicoGreen dsDNA assay kit (Life Technologies, Carlsbad, CA). GAG content was determined using the dimethylmethylene blue (DMMB) assay, and collagen content quantified via the p-diaminobenzaldehyde/chloramine-T assay for hydroxyproline (OHP). GAG and collagen content were normalized to sample wet weight and DNA content.

For histologic assessment of matrix distribution at each time point, medium and large DAPS were fixed in 10% neutral buffered formalin (Sigma-Aldrich), processed through paraffin, and sectioned in the sagittal plane to 7 μm thickness. Sections were stained with either Alcian blue for sulfated GAG or picrosirius red for collagen. Immunohistochemistry was performed for collagen I (EMD Millipore, AB749P, Billerica, MA), collagen II (DSHB, II-II6B3, Iowa City, Iowa), and chondroitin sulfate (DSHB, 9BA12). Follow rehydration, slides were serially incubated in proteinase K (Dako Glostrup, Denmark) for 10 minutes at room temperature (RT), 3% hydrogen peroxide for 10 minutes at RT, horse serum for 30 minutes at RT (Vectastain ABC Universal Kit, Vector Laboratories, Burlingame, CA), and primary antibody (10 μg/mL) overnight at 4°C. Secondary detection was achieved using the Vectastain Elite ABC Universal HRP Kit (PK-6200, Vector Laboratories, Burlingame, CA) and visualized using 3,3'-diaminobenzidine (Millipore, Billerica, MA).

2.5 Magnetic Resonance Imaging

T2 mapping is a non-invasive, clinically relevant metric for assessing disc composition and health, as it is strongly correlated with tissue water and proteoglycan content [29,30]. A 4.7T MRI spectrometer (Magnex Scientific Limited, Abington, United Kingdom) was used to obtain multi-slice, multi-echo images of *in vitro* cultured DAPS (three 0.5 mm thick slices, 16 echoes, echo time/repetition time = 20 ms/2,000 ms, 4 averages, 128x64 data matrix). A 15 mm by 7.5 mm field of view was utilized for medium DAPS, and a 15 mm by 30 mm field of view was utilized for large DAPS, yielding in-plane resolution of 117 microns. The AF and NP regions were manually contoured, and the mean T2 relaxation time was calculated for each region using custom MATLAB software [31].

2.6 Subcutaneous Implantation in Rats

Eight medium and eight large DAPS were fabricated as described in Section 2.1 and pre-cultured for 5 weeks in CM+. The 5 week pre-culture duration was selected to match our previous subcutaneous implantation studies on small sized DAPS [20]. DAPS were then implanted into the dorsal subcutaneous space of athymic retired breeder rats (n=11, Hsd:RH-Foxn1^{rnu}, male, 9-10 months, 490±40g, Envigo, Branchburg, NJ), with institutional approval

and according to the guidelines prescribed by the NIH Guide for Care and Use of Laboratory Animals. Rats were anesthetized with isoflurane and either one (for large DAPS) or three (for medium DAPS) dorsal pockets were opened using sharp and blunt dissection. One DAPS was inserted into each pocket, and the incision closed with 3-0 suture. Rats were returned to normal cage activity after the procedure. and administered 0.1 mg/kg buprenorphine twice per day for three days for analgesia, and 15 mg/kg of cefazolin for antibiotic prophylaxis, via subcutaneous injection. Rats were euthanized 5 weeks post-implantation. Four DAPS of each size were halved following excision from the subcutaneous pockets. One half-DAPS was utilized for NP cell viability and AF cell metabolic activity assays as described in section 2.2. The remaining half-DAPS was utilized for quantification of DNA, collagen and GAG content as detailed in section 2.4. Two DAPS per size were processed for histological evaluation of extracellular matrix distribution, as described in section 2.4.

2.7 Statistical Analyses

Statistical analyses were conducted in Prism (Graph Pad Software Inc., La Jolla, CA), with significance defined as $p < 0.05$. All data are shown as mean ± standard deviation. Two-way analyses of variance (ANOVA) with Tukey's post-hoc tests were used to establish significant differences in cell viability (live/dead cell counts and MTT absorbance), biochemistry (GAG, DNA and collagen), MRI T2 values, and mechanical properties between medium and large DAPS and between the 5, 10 and 15 weeks *in vitro* culture time points. For the subcutaneous implantation study, two-way ANOVA with Tukey's post-hoc tests were used to establish significant differences in cell viability and biochemistry for medium and large DAPS between 5 weeks of pre-culture (PC) and subcutaneous implantation (SQ).

Pearson correlation coefficients (PCC) were calculated in R (corr.test function, R-project.org) between MRI (AF and NP T2), biochemistry (AF and NP GAG and collagen) and mechanical properties (toe and linear region modulus, transition strain and ROM) for medium and large DAPS over the 15 week *in vitro* culture duration. A matrix of the average ratio of the correlation coefficients between medium and large DAPS was calculated as $[(PCC_{medium}/PCC_{large}) + (PCC_{large}/PCC_{medium})]/2$. A ratio close to 1 indicates similar correlation coefficients at each length scale, and negative ratios indicate a change in sign of the correlation coefficient across length scales.

3. Results

3.1 Viability and Metabolic Activity

Medium and large DAPS were successfully fabricated and cultured for up to 15 weeks *in vitro* (Figure 1). In medium DAPS, cell viability in the NP region as a whole was maintained over the 15-week culture duration (Figure 2A); however, a significant reduction in cell number in the center region of the NP was observed between 5 and 10 weeks of culture. Mean percent viability of cells in the center of the NP remained high, however, stabilizing at 79.1% at 15 weeks. In contrast, for large DAPS, cell number significantly decreased across the entire NP region. Percent viability decreased from a mean of 88.5% at 5 weeks to 63.2% after 15 weeks. This was primarily due to reductions in cell number and percent viability in

the central NP region of these large DAPS (Figure 2B), with percent viability in the center reaching a low of 30% after 15 weeks (Figure 2C).

AF cell metabolic activity, as measured via the MTT assay, was similar between medium and large DAPS at 5 weeks. At 10 and 15 weeks, however, MTT absorbance normalized to wet weight in the AF region was significantly higher in medium DAPS compared to large DAPS (Figure 2D). No significant differences in normalized MTT absorbance were observed for the AF region of medium or large DAPS between 10 and 15 weeks of culture. DAPI staining (Figure 2E) illustrated the presence of cell nuclei between the PCL layers of the DAPS for the medium and large AF over the 15-week culture duration, however, there was little evidence of AF cell infiltration into the individual PCL layers over this time course.

Based on DNA measurements (estimating ~7 pg DNA per cell [32]), and DAPS volume, the average cell densities (Figure S1) during *in vitro* culture in the NP were approximately 50,000 cells/mm^3 and 20,000 cells/mm^3 for medium and large DAPS, respectively. In the AF region, cell density increased over time in culture, with approximate cell densities ranging from 45,000 cells/mm^3 (5 weeks) to 70,000 cells/mm^3 (15 weeks) in medium DAPS, and from 25,000 cells/mm^3 (5 weeks) to 30,000 cells/mm^3 (15 weeks) in large DAPS.

3.2 Mechanical Properties

Representative compressive stress-strain curves for medium (Figure 3A) and large (Figure 3B) DAPS illustrate functional maturation with increasing duration of *in vitro* culture, with medium DAPS maturing more rapidly than large DAPS. For medium DAPS, no significant differences in toe region modulus, linear region modulus, ROM, or transition strain were observed over the 15-week culture duration. Toe region modulus (Figure 3C) significantly increased in large DAPS between 5 weeks and 15 weeks of culture but there were no significant differences in linear region modulus (Figure 3D) in large DAPS over this time period. In large DAPS, ROM was significantly reduced after 15 weeks compared to 5 and 10 weeks, while transition strain was significantly reduced after 15 weeks compared to 5 weeks. ROM was significantly lower in medium size DAPS at the 5 and 10-week time points, but no other significant differences in mechanical properties between size scales were observed.

3.3 Composition and Matrix Distribution

NP GAG content, when normalized to wet weight (Figure 4A) or DNA content (Figure 4B), was not significantly affected by culture duration for medium or large DAPS. NP GAG normalized to NP wet weight was significantly higher at all experimental time points in medium DAPS compared to large DAPS. However, there were no significant differences in GAG per DNA in the NP region between size scales at any time point. The maximal NP GAG content achieved was 3.0% ww and 1.5% ww for medium and large DAPS, respectively. NP collagen content normalized to wet weight (Figure 4C) significantly increased with increasing duration of culture for both size scales, although NP collagen was significantly higher in medium DAPS compared to large DAPS at all experimental time

points. NP collagen content per DNA (Figure 4D) was not significantly altered by size scale or culture duration. The maximal NP collagen content achieved was 2.0% ww for medium DAPS and 1.1% ww for large DAPS.

AF GAG content, normalized to wet weight (Figure 4E) or DNA content (Figure 4F), significantly increased with increasing culture duration for both medium and large DAPS. AF GAG content normalized to wet weight was higher in medium DAPS compared to large DAPS at 10 and 15 weeks. AF GAG content normalized to DNA was significantly higher in medium DAPS compared to large DAPS only at the 15-week time point. The maximal AF GAG content was 2.4% ww in medium DAPS and 1.2% ww in large DAPS. AF collagen content, normalized to either wet weight (Figure 4G) or DNA content (Figure 4F), significantly increased over the 15-week culture duration for both size scales, reaching maximal values of 1.43% ww for medium DAPS and 1.0% ww for large DAPS. When normalized to wet weight, AF collagen content was significantly higher in medium DAPS compared to large DAPS at the 10 and 15-week time points. There were no significant differences at any time point between size scales for AF collagen content per DNA.

Sagittal histological sections of medium DAPS (Figure 5) at each experimental time point show increasing staining for both proteoglycans and collagens, particularly in the AF region. Inhomogeneity in matrix staining was observed in medium DAPS, with more intense staining observed along the periphery of the NP and AF. Increased deposition of proteoglycan and collagen matrix over the 15-week culture duration was also seen in large DAPS (Figure 6). However, in these larger constructs, the inhomogeneity in matrix distribution from the periphery to the center of the construct was exacerbated compared to medium DAPS.

3.4 Quantitative MRI T2 Mapping

In general, we have found that T2 values are reduced as the DAPS mature during *in vitro* culture and increasing amounts of matrix are deposited [20]. Representative T2 maps for medium and large DAPS at each time point (Figure 7A), demonstrate the inhomogeneity in T2 values in the NP region in large DAPS compared to medium DAPS, corresponding to the low matrix content in the central NP of the large DAPS, compared to the homogenous NP matrix in medium DAPS. T2 values in both the AF and NP regions generally decreased with increasing construct maturation and matrix deposition, as expected. Inhomogeneity in AF T2 values was evident in both medium and large DAPS over the 15-week culture duration, with lower T2 values at the periphery of the construct where more robust matrix formation had occurred. NP T2 values (Figure 7B) were not significantly affected by the duration of culture at either size scale, however, T2 values in the NP of medium DAPS were significantly lower than NP T2 values of large DAPS after 5 and 10 weeks. AF T2 values (Figure 7C) significantly decreased with increasing culture duration for both medium and large-size DAPS. AF T2 values were significantly lower in medium DAPS compared to larger DAPS at all experimental time points.

3.5 Correlation Analyses

To develop structure/function relationships for these maturing DAPS constructs, a correlation analysis relating all factors was performed. For large DAPS (Table S1), AF T2 significantly correlated with AF collagen (PCC = −0.76) and AF GAG content (PCC = −0.82). No significant correlations were found for NP T2, and no significant correlations between mechanical properties and biochemical content or MRI T2 were found for large DAPS. Stronger correlations between variables were generally found for medium DAPS compared to large DAPS. In medium DAPS (Table S2), AF T2 was significantly correlated with toe modulus (PCC = −0.86), and NP T2 was significantly correlated with AF GAG (PCC = 0.80) and collagen content (PCC = 0.75). AF GAG content was also significantly correlated with ROM (PCC = 0.76) for medium DAPS. The average ratio of correlation coefficients (Table S3) demonstrated a change in sign of the correlation coefficient between size scales for correlations with NP T2, linear modulus and ROM.

3.6 Subcutaneous Implantation

Following subcutaneous implantation for 5 weeks, NP cell viability (Figure 8A) was significantly reduced compared to pre-implantation levels in both medium and large DAPS. AF cell metabolic activity (Figure 8B) significantly increased from pre-implantation levels in medium DAPS, but was unchanged in large DAPS. Based on DNA quantification (Figure S1), cell density after subcutaneous implantation was reduced overall to approximately 10,000 cells/mm^3 in the NP and 1,000 cells/mm^3 in the AF for medium DAPS. For large DAPS after subcutaneous implantation, cell density was approximately 2,000 cells/mm^3 in the NP and 5,000 cells/mm^3 in the AF.

NP GAG content (Figure 8C) significantly decreased following subcutaneous implantation in both medium and large DAPS compared to pre-implantation values, while NP collagen content (Figure 8E) significantly increased in medium DAPS and was unchanged in large DAPS. AF GAG content (Figure 8D) and collagen content (Figure 8F) remained at pre-implantation values at both size scales. Medium DAPS outperformed the large DAPS following the transition to the *in vivo* environment with respect to NP cell viability, AF cell metabolic activity, and NP collagen content. Quantitative analysis of matrix composition was confirmed via Alcian blue (Figure 8G) and Picrosirius red (Figure 8H) stained sections, which highlighted the loss of proteoglycan staining in the NP region for medium and large DAPS, and the increase in collagen staining in the NP of the medium DAPS. The extent of fibrous capsule formation around the DAPS was also greater in the large DAPS compared to the medium DAPS.

4. Discussion

IVD tissue engineering is a promising treatment strategy for end-stage disc degeneration, with the potential to restore structure and function compared with standard spinal fusion techniques. While several groups have developed composite engineered IVDs composed of tissue engineered NP and AF analogs, the size of such constructs remain a fraction of the size of human cervical or lumbar IVDs [11,13-17]. In this study, we fabricated and characterized tissue-engineered IVDs at two length scales – a medium-sized construct 10

mm in diameter and 3 mm thick, and a larger construct 20 mm in diameter and 6 mm thick. While the medium DAPS were sized for evaluation in the rabbit lumbar IVD, the large DAPS were designed for use in the goat cervical IVD, which has comparable dimensions to the human cervical IVD [33]. To our knowledge, the large DAPS are the first whole engineered IVD constructs to be fabricated at clinically relevant length scales.

In this study, while large DAPS matured functionally and compositionally over the duration of *in vitro* culture, they were outperformed by the medium DAPS in nearly all outcome measures. Additionally, while matrix production and cell viability were robust along the periphery of the large size DAPS, there were significant deficiencies in viability and matrix content in the central region. Heterogeneity in viability and matrix distribution is commonly observed in engineered cartilage and IVD constructs, even at smaller length scales, and is governed by diffusional gradients of media components, primarily glucose, that occur during *in vitro* culture [26,34-40]. As a consequence, biochemical content in the NP and AF regions of the DAPS did not reach native levels of the human, goat or rabbit IVD, with the exception of NP collagen content (Table 1) [28,41]. Nonetheless, construct GAG and collagen were within the range of previously reported tissue engineered IVD compositions [13,16,19,28,41]. Similar maximal compressive mechanical properties were achieved at both size scales (0.23 MPa toe region modulus and 2.5 MPa linear region modulus), but these too did not reach levels of the native human IVD (9 MPa) [28]. The linear region modulus was unchanged over the culture duration at both size scales, likely as it is largely dominated by the mechanical properties of the PCL itself [21].

Following subcutaneous implantation, medium DAPS generally outperformed the large DAPS, maintaining better cell viability, AF cell metabolic activity, and NP collagen content than the large DAPS. At both size scales, subcutaneous implantation had no negative effect on the AF region of the DAPS, but led to significant reductions in cell viability and proteoglycan content in the NP region. This loss of proteoglycan content in tissue-engineered constructs following subcutaneous implantation has been observed previously by our group in small DAPS sized for the rat caudal disc space, as well as by others in engineered cartilage tissues [20,42]. However, the results in the subcutaneous space may not be representative of the response following implantation in the disc space, as we have previously shown maintenance of DAPS matrix in a rat caudal disc replacement model [21]. Previous work has shown matrix accumulation in engineered IVDs following subcutaneous implantation in mice and rats [16,43], however, these constructs were not pre-cultured, and were therefore implanted in an immature state compared to the constructs evaluated in the current study. In the future, a trajectory based tissue engineering approach could be utilized to identify the pre-culture duration prior to implantation needed to optimize *in vivo* outcomes [44].

Structure-function analyses illustrated a greater number of significant correlations between outcome measures (MRI T2, biochemistry and mechanical properties) in medium DAPS compared with large DAPS. In medium DAPS, biochemistry and T2 values were significantly correlated with mechanical properties, however in large DAPS, there were no significant correlations between biochemistry or T2 and mechanical properties. This suggests that matrix accumulation during culture altered the mechanical function of the

medium DAPS but not the large DAPS, likely due to the inhomogeneity in matrix distribution in the large DAPS. Similarly, previous cartilage tissue engineering work has illustrated that matrix inhomogeneity can influence construct mechanical properties and structure-function correlations [38,45]. Composition-function relationships between biochemistry, MRI T2 and mechanical properties have been shown to exist in the native IVD [30]. Recapitulating these correlations in an engineered construct can therefore provide a quantitative benchmark for the successful fabrication of an engineered IVD.

The results from this work demonstrate the challenge of tissue-engineering an anatomically sized IVD that recapitulates the scale and avascular nature of the mature native tissue [46]. During development, the size of the IVD scales with growth, and immature IVDs have a greater supply of nutrients via vascularization of the AF, which regresses with increasing age as the IVD develops [47]. Lacking an analog to development *in vitro,* nutrient supply to large-scale tissue engineered IVDs poses a significant challenge, particularly as a growing construct has a greater metabolic demand than the mature native IVD, whose cells function to maintain, rather than establish, the functional ECM. Engineering strategies will therefore need to be employed in future work to enhance viability and matrix distribution in large-size DAPS, particularly when transitioning to the use of more clinically relevant cell types such as mesenchymal stem cells, which are more sensitive to nutrient deprivation than disc cells [40,48].

Improvements in nutrient transport into the central regions of large, tissue-engineered cartilage constructs have been previously achieved via the inclusion of channels through the construct depth, and led to enhanced cell viability and matrix deposition during culture [49-51]. Such channels could be readily incorporated into the NP region of the DAPS at large size scales to enhance nutrient transport. In the AF region, the composition of the electrospun layers could be altered by incorporating fibers of poly(ethylene oxide), which is water soluble, within and amongst the PCL fibers to increase the porosity of the AF layers and enhance cell infiltration within each layer, thereby potentially improving AF matrix distribution [52]. We have previously shown that such approaches, over the long term, increase the functional properties and matrix content of fibrous tissue analogs [53]. Alterations to the culture media may also enhance the homogeneity of matrix distribution in the large DAPS. Previous work has shown that supplementation of chemically defined media with latent TGF-β increases the uniformity of matrix biosynthesis throughout engineered cartilage tissues, while media supplemented with active TGF-β caused heterogeneous matrix and cell distribution, concentrated at the periphery, similar to that observed in the current study [37]. Finally, culture of DAPS constructs in a bioreactor that applies physiological loading may also be a promising method for improving cell viability, matrix production and mechanical properties by enhancing nutrient transport and providing direct cellular stimulation [54]. For instance, culture in a compression bioreactor enhanced the mechanical properties and biochemical content of tissue-engineered discs composed of collagen and alginate, and improved the properties of hydrogels seeded with chondrocytes or mesenchymal stem cells for cartilage tissue engineering [39,55-57].

5. Conclusions

In conclusion, we fabricated and evaluated the maturation of tissue-engineered IVDs at clinically relevant size scales during *in vitro* culture and following *in vivo* subcutaneous implantation. While medium DAPS outperformed large DAPS, those sized for the goat and human cervical disc space did functionally and compositionally mature with increasing culture duration. Future work will seek to optimize the properties of these large size DAPS *in vitro*, as well as to evaluate the performance of both sized constructs in pre-clinical animal models to advance their clinical translation.

Supplementary Material

Refer to Web version on PubMed Central for supplementary material.

Acknowledgements

This work was supported by the Department of Veterans Affairs (IK2 RX001476 & I01 RX002274) and the Penn Center for Musculoskeletal Disorders (National Institutes of Health P30 AR069619). The authors would like to acknowledge Debra Pawlowski and Jeffrey House from the Corporal Michael J. Crescenz VA Medical Center Animal Research Facility for their assistance with the animal studies.

Role of the Funding Source

The content is solely the responsibility of the authors and does not necessarily represent the official views of the Department of Veteran's Affairs. No funding source had a role in the study design, collection, analysis and interpretation of data, writing of the manuscript, or the decision to submit the manuscript for publication.

References

[1]. Cassidy J, Hiltner A, Hierarchical structure of the intervertebral disc, Connect. Tissue Res 23 (1989) 75–88. [PubMed: 2632144]

[2]. Humzah M, Soames R, Human intervertebral disc: structure and function, Anat. Rec 220 (1988) 337–356. [PubMed: 3289416]

[3]. American Academy of Orthopaedic Surgeons, The Burden of Musculoskeletal Diseases in the United States, Academy of Orthopaedic Surgeons, Rosemont, IL, 2008.

[4]. Urban JPG, Roberts S, Degeneration of the intervertebral disc, Arthritis Res. Ther 5 (2003) 120–130. [PubMed: 12723977]

[5]. Murray CJL, Vos T, Lozano R, Disability-adjusted life years (DALYs) for 291 diseases and injuries in 21 regions, 1990-2010: a systematic analysis for the Global Burden of Disease Study 2010., Lancet. 380 (2012) 2197–223. doi:10.1016/S0140-6736(12)61689-4. [PubMed: 23245608]

[6]. Ma V, Chan L, Carruthers K, The Incidence, Prevalence, Costs and Impact on Disability of Common Conditions Requiring Rehabilitation in the US: Stroke, Spinal Cord Injury, Traumatic Brain Injury, Multiple Sclerosis, Osteoarthritis, Rheumatoid Arthritis, Limb Loss, and Back Pain, Arch Phys Med Rehabil. 95 (2014) 986–995. doi:10.1016/j.apmr.2013.10.032.The. [PubMed: 24462839]

[7]. Saltychev M, Eskola M, Laimi K, Lumbar fusion compared with conservative treatment in patients with chronic low back pain, Int. J. Rehabil. Res 37 (2014) 2–8. doi:10.1097/MRR.0b013e328363ba4b. [PubMed: 23820296]

[8]. Ghiselli G, Wang JC, Bhatia NN, Hsu WK, Dawson EG, Adjacent segment degeneration in the lumbar spine., J. Bone Joint Surg. Am 86–A (2004) 1497–503.

[9]. Harrop JS, a Youssef J, Maltenfort M, Vorwald P, Jabbour P, Bono CM, Goldfarb N, Vaccaro AR, Hilibrand AS, Lumbar adjacent segment degeneration and disease after arthrodesis and total disc

arthroplasty., Spine (Phila. Pa. 1976). 33 (2008) 1701–1707. doi:10.1097/BRS.0b013e31817bb956. [PubMed: 18594464]

[10]. Freeman BJC, Davenport J, Total disc replacement in the lumbar spine: A systematic review of the literature, Eur. Spine J 15 (2006). doi:10.1007/s00586-006-0186-9.

[11]. Bowles RD, Gebhard HH, Härtl R, Bonassar LJ, Tissue-engineered intervertebral discs produce new matrix, maintain disc height, and restore biomechanical function to the rodent spine., Proc. Natl. Acad. Sci. U. S. A 108 (2011) 13106–11. doi:10.1073/pnas.1107094108. [PubMed: 21808048]

[12]. Nesti LJ, Li W-JJ, Shanti RM, Jiang YJ, Jackson W, Freedman BA, Kuklo TR, Giuliani JR, Tuan RS, Intervertebral disc tissue engineering using a novel hyaluronic acid-nanofibrous scaffold (HANFS) amalgam., Tissue Eng Part A. 14 (2008) 1527–1537. doi:10.1089/ten.tea.2008.0215. [PubMed: 18707229]

[13]. Park S-H, Gil ES, Cho H, Mandal BB, Tien LW, Min B-H, Kaplan DL, Intervertebral disk tissue engineering using biphasic silk composite scaffolds., Tissue Eng. Part A 18 (2012) 447–58. doi:10.1089/ten.TEA.2011.0195. [PubMed: 21919790]

[14]. Lazebnik M, M S, Glatt P, Friis L, Berkland C, Detamore M, Biomimetic method for combining the nucleus pulposus and annulus fibrosus, J. Tissue Eng. Regen. Med 5 (2011) e179–e187. doi:10.1080/01425690701737481. [PubMed: 21774081]

[15]. Choy ATH, Chan BP, A Structurally and Functionally Biomimetic Biphasic Scaffold for Intervertebral Disc Tissue Engineering, PLoS One. 10 (2015) e0131827. doi:10.1371/journal.pone.0131827. [PubMed: 26115332]

[16]. Mizuno H, Roy AK, Zaporojan V, a Vacanti C, Ueda M, Bonassar LJ, Biomechanical and biochemical characterization of composite tissue-engineered intervertebral discs., Biomaterials. 27 (2006) 362–70. doi:10.1016/j.biomaterials.2005.06.042. [PubMed: 16165204]

[17]. Iu J, Massicotte E, Li S-Q, Hurtig MB, Toyserkani E, Santerre JP, Kandel R, In Vitro Generated Intervertebral Discs: Towards Engineering Tissue Integration, Tissue Eng. Part A. (2017) ten.TEA.2016.0433. doi:10.1089/ten.TEA.2016.0433.

[18]. Moriguchi Y, Navarro R, Grunert P, Mojica J, Hudson K, Khair T, Alimi M, Bonassar L, Hartl R, Total Disc Replacement Using Tissue Engineered Intervertebral Discs In An In-vivo Beagle Model, PLoS One. 12 (2017) 1–18.

[19]. Nerurkar NL, Sen S, Huang AH, Elliott DM, Mauck RL, Engineered disc-like angle-ply structures for intervertebral disc replacement., Spine (Phila. Pa. 1976). 35 (2010) 867–73. doi:10.1097/BRS.0b013e3181d74414. [PubMed: 20354467]

[20]. Martin JT, Gullbrand SE, Mohanraj BG, Ashinsky BG, Kim DH, Ikuta K, Elliott DM, Smith LJ, Mauck RL, Smith HE, Optimization of pre-culture conditions to maximize the in vivo performance of cell-seeded engineered intervertebral discs, Tissue Eng. Part A 23 (2017) 923–234. doi:10.1089/ten.TEA.2016.0491. [PubMed: 28426371]

[21]. Martin JT, Gullbrand SE, Kim D, Ikuta K, Pfeifer CG, Ashinsky BG, Smith LJ, Elliott DM, Smith HE, Mauck RL, In Vitro Maturation and In Vivo Integration and Function of an Engineered Cell-Seeded Disc-like Angle Ply Structure (DAPS) for Total Disc Arthroplasty, Sci. Rep 7 (2017) 15765. [PubMed: 29150639]

[22]. O'Connell GD, Vresilovic EJ, Elliott DM, Connell GDO, Comparison of animals used in disc research to human lumbar disc geometry., Spine (Phila. Pa. 1976). 32 (2007) 328–33. doi:10.1097/01.brs.0000253961.40910.c1. [PubMed: 17268264]

[23]. Qin J, He X, Wang D, Qi P, Guo L, Huang S, Cai X, Li H, Wang R, Artificial Cervical Vertebra and Intervertebral Complex Replacement through the Anterior Approach in Animal Model: A Biomechanical and In Vivo Evaluation of a Successful Goat Model, PLoS One. 7 (2012). doi:10.1371/journal.pone.0052910.

[24]. Busscher I, Ploegmakers JJW, Verkerke GJ, Veldhuizen AG, Comparative anatomical dimensions of the complete human and porcine spine., Eur. Spine J 19 (2010) 1104–14. doi:10.1007/s00586-010-1326-9. [PubMed: 20186441]

[25]. Nerurkar NL, Elliott DM, Mauck RL, Mechanics of oriented electrospun nanofibrous scaffolds for annulus fibrosus tissue engineering., J. Orthop. Res 25 (2007) 1018–28. doi:10.1002/jor.20384. [PubMed: 17457824]

[26]. Farrell MJ, Comeau ES, Mauck RL, Mesenchymal stem cells produce functional cartilage matrix in three-dimensional culture in regions of optimal nutrient supply., Eur. Cell. Mater 23 (2012) 425–40. [PubMed: 22684531]

[27]. Martin JT, Gorth DJ, Beattie EE, Harfe BD, Smith LJ, Elliott DM, Needle puncture injury causes acute and long-term mechanical deficiency in a mouse model of intervertebral disc degeneration, J. Orthop. Res 31 (2013) 1276–1282. doi:10.1002/jor.22355. [PubMed: 23553925]

[28]. Beckstein JC, Sen S, Schaer TP, Vresilovic EJ, Elliott DM, Comparison of animal discs used in disc research to human lumbar disc: axial compression mechanics and glycosaminoglycan content., Spine (Phila. Pa. 1976). 33 (2008) E166–73. [PubMed: 18344845]

[29]. Mwale F, Iatridis JC, Antoniou J, Quantitative MRI as a diagnostic tool of intervertebral disc matrix composition and integrity, Eur. Spine J 17 (2008) 432–440. doi:10.1007/s00586-008-0744-4.

[30]. Gullbrand SE, Ashinsky BG, Martin JT, Pickup S, Smith LJ, Mauck RL, Smith HE, Correlations between quantitative T2 and T1ρ MRI, mechanical properties and biochemical composition in a rabbit lumbar intervertebral disc degeneration model, J. Orthop. Res (2016) 1–25. doi:10.1002/jor.23269.

[31]. Martin JT, Collins CM, Ikuta K, Mauck RL, Elliott DM, Zhang Y, Anderson DG, Vaccaro AR, Albert TJ, Arlet V, Smith HE, Population average T2 MRI maps reveal quantitative regional transformations in the degenerating rabbit intervertebral disc that vary by lumbar level, J. Orthop. Res 33 (2015) 140–148. doi:10.1002/jor.22737. [PubMed: 25273831]

[32]. Lee GM, Thornthwaite JT, Rasch EM, Picogram per cell determination of DNA by flow cytofluorometry, Anal. Biochem 137 (1984) 221–226. doi:10.1016/0003-2697(84)90374-9. [PubMed: 6731800]

[33]. Connell GDO, Vresilovic EJ, Elliott DM, Comparison of Animals Used in Disc Research to Human Lumbar Disc Geometry, 32 (2007) 328–333.

[34]. Saxena V, Kim M, Keah NM, Neuwirth AL, Stoeckl BD, Bickard K, Restle DJ, Salowe R, Wang MY, Steinberg DR, Mauck RL, Anatomic Mesenchymal Stem Cell-Based Engineered Cartilage Constructs for Biologic Total Joint Replacement, Tissue Eng. Part A 22 (2016) 386–395. doi:10.1089/ten.tea.2015.0384. [PubMed: 26871863]

[35]. Vedicherla S, Buckley CT, In vitro extracellular matrix accumulation of nasal and articular chondrocytes for intervertebral disc repair, Tissue Cell. in press (2017). doi:10.1016/j.limno.2010.12.003.

[36]. Heywood HK, Bader DL, a Lee D, Glucose concentration and medium volume influence cell viability and glycosaminoglycan synthesis in chondrocyte-seeded alginate constructs., Tissue Eng. 12 (2006) 3487–96. doi:10.1089/ten.2006.12.3487. [PubMed: 17518685]

[37]. Albro MB, Nims RJ, Durney KM, Cigan AD, Shim JJ, Vunjak-Novakovic G, Hung CT, Ateshian GA, Heterogeneous engineered cartilage growth results from gradients of media-supplemented active TGF-β and is ameliorated by the alternative supplementation of latent TGF-β, Biomaterials. 77 (2016) 173–185. doi:10.1016/j.biomaterials.2015.10.018. [PubMed: 26599624]

[38]. Buckley CT, Meyer EG, Kelly DJ, The Influence of Construct Scale on the Composition and Functional Properties of Cartilaginous Tissues Engineered Using Bone Marrow-Derived Mesenchymal Stem Cells, Tissue Eng. Part A 18 (2012) 382–396. doi:10.1089/ten.tea.2011.0145. [PubMed: 21919793]

[39]. Mauck RL, Wang CCB, Oswald ES, Ateshian GA, Hung CT, The role of cell seeding density and nutrient supply for articular cartilage tissue engineering with deformational loading, Osteoarthr. Cartil 11 (2003) 879–890. doi:10.1016/j.joca.2003.08.006.

[40]. Farrell MJ, Shin JI, Smith LJ, Mauck RL, Functional consequences of glucose and oxygen deprivation on engineered mesenchymal stem cell-based cartilage constructs, Osteoarthr. Cartil 23 (2015) 134–142. doi:10.1016/j.joca.2014.09.012.

[41]. Showalter BL, Beckstein JC, Martin JT, Elizabeth E, Orías AAE, Schaer TP, Edward J, Elliott DM, Comparison of Animal Discs Used in Disc Research to Human Lumbar Disc: Torsion Mechanics and Collagen Content, Spine (Phila. Pa. 1976). 37 (2012) 1–17. doi:10.1097/BRS.0b013e31824d911c.Comparison.

[42]. Vinardell T, Sheehy EJ, Buckley CT, Kelly DJ, A Comparison of the Functionality and In Vivo Phenotypic Stability of Cartilaginous Tissues Engineered from Different Stem Cell Sources, Tissue Eng. Part A 18 (2012) 1161–1170. doi:10.1089/ten.tea.2011.0544. [PubMed: 22429262]

[43]. Zhuang Y, Huang B, Li CQ, Liu LT, Pan Y, Zheng WJ, Luo G, Zhou Y, Construction of tissue-engineered composite intervertebral disc and preliminary morphological and biochemical evaluation, Biochem. Biophys. Res. Commun 407 (2011) 327–332. doi:10.1016/j.bbrc.2011.03.015. [PubMed: 21382343]

[44]. Fisher MB, Henning EA, Söegaard NB, Dodge GR, Steinberg DR, Mauck RL, Maximizing cartilage formation and integration via a trajectory- based tissue engineering approach, Biomaterials. 35 (2014) 2140–2148. doi:10.1016/j.biomaterials.2013.11.031. [PubMed: 24314553]

[45]. Kelly DJ, Prendergast PJ, Effect of a degraded core on the mechanical behaviour of tissue engineered cartilage constructs a pro elastic finite element analysis, Med. Biol. Eng. Comput 42 (2004) 9–13. [PubMed: 14977217]

[46]. Urban JPG, Smith S, Fairbank JCT, Nutrition of the Intervertebral Disc, 29 (2004) 2700–2709.

[47]. Smith LJ, Elliott DM, Formation of lamellar cross bridges in the annulus fibrosus of the intervertebral disc is a consequence of vascular regression, Matrix Biol. 30 (2011) 267–274. doi:10.1016/j.matbio.2011.03.009. [PubMed: 21504791]

[48]. Turner SA, Wright KT, Jones PN, Balain B, Roberts S, Temporal Analyses of the Response of Intervertebral Disc Cells and Mesenchymal Stem Cells to Nutrient Deprivation, Stem Cells Int. 2016 (2016) 1–13. doi:10.1155/2016/5415901.

[49]. Nims RJ, Cigan AD, Albro MB, Vunjak-Novakovic G, Hung CT, Ateshian G. a., Matrix Production in Large Engineered Cartilage Constructs Is Enhanced by Nutrient Channels and Excess Media Supply, Tissue Eng. Part C Methods 21 (2015) 150403125943008. doi:10.1089/ten.tec.2014.0451.

[50]. Kim M, Farrell MJ, Steinberg DR, Burdick JA, Mauck RL, Enhanced nutrient transport improves the depth-dependent properties of tri-layered engineered cartilage constructs with zonal co-culture of chondrocytes and MSCs, Acta Biomater. 58 (2017) 1–11. doi:10.1016/j.actbio.2017.06.025. [PubMed: 28629894]

[51]. Buckley CT, Thorpe SD, Kelly DJ, Engineering of large cartilaginous tissues through the use of microchanneled hydrogels and rotational culture., Tissue Eng. Part A 15 (2009) 3213–20. doi:10.1089/ten.TEA.2008.0531. [PubMed: 19374490]

[52]. Baker BM, Gee AO, Metter RB, Nathan AS, Marklein RA, Burdick JA, Mauck RL, The potential to improve cell infiltration in composite fiber-aligned electrospun scaffolds by the selective removal of sacrificial fibers, Biomaterials. 29 (2008) 2348–2358. doi:10.1016/j.biomaterials.2008.01.032. [PubMed: 18313138]

[53]. Baker BM, Shah RP, Silverstein AM, Esterhai JL, a Burdick J, Mauck RL, Sacrificial nanofibrous composites provide instruction without impediment and enable functional tissue formation., Proc. Natl. Acad. Sci. U. S. A 109 (2012) 14176–81. doi:10.1073/pnas.1206962109. [PubMed: 22872864]

[54]. Huang AH, Farrell MJ, Mauck RL, Mechanics and mechanobiology of mesenchymal stem cell-based engineered cartilage., J. Biomech 43 (2010) 128–36. doi:10.1016/j.jbiomech.2009.09.018. [PubMed: 19828149]

[55]. Hudson KD, Mozia RI, Bonassar LJ, Dose-Dependent Response of Tissue-Engineered Intervertebral Discs to Dynamic Unconfined Compressive Loading., Tissue Eng. Part A 21 (2015) 564–572. doi:10.1089/ten.tea.2014.0174. [PubMed: 25277703]

[56]. Huang A, Farrell M, Kim M, Mauck R, Long-term dynamic loading improves the mechanical properties of chondrogenic mesenchymal stem cell-laden hydrogels, Eur. Cell. Mater (2010) 72–85.

[57]. Mauck RL, Soltz MA, Wang CCB, Wong DD, Chao PG, Ateshian GA, Functional Tissue Engineering of Articular Cartilage Through Dynamic Loading of, 122 (2000).

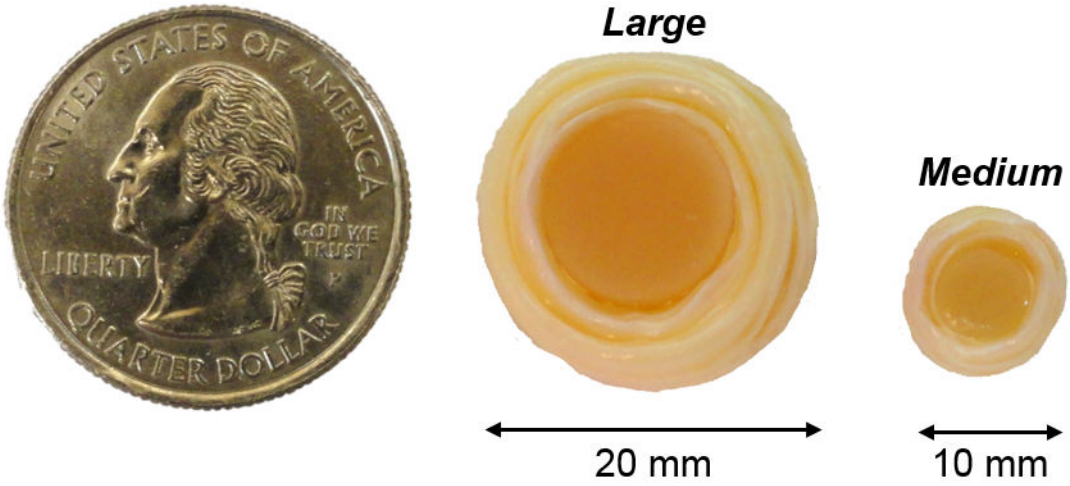

Figure 1. Fabrication of DAPS at clinically relevant size scales.

To-scale photograph of medium and large DAPS compared to the size of a US quarter.

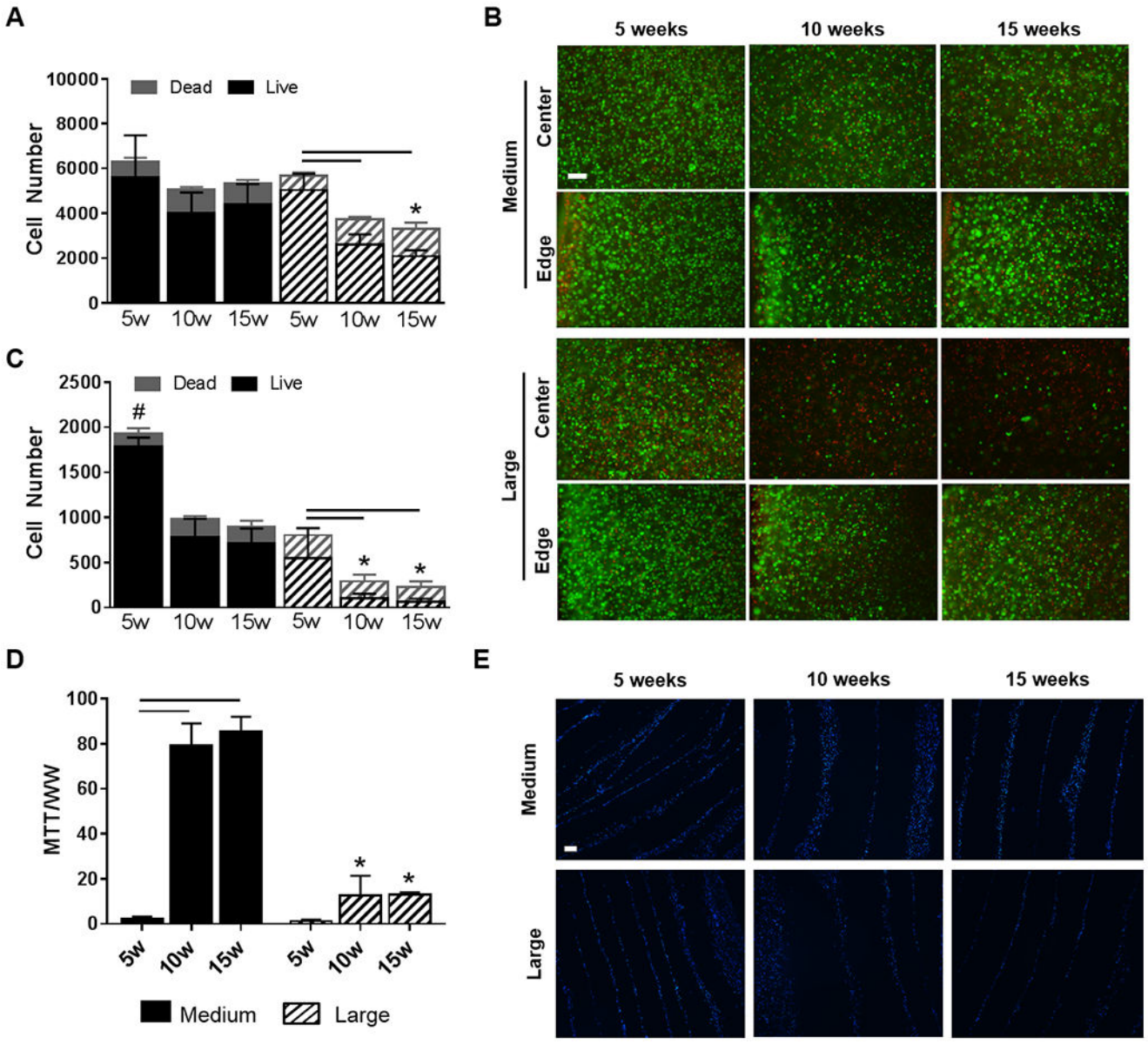

Figure 2. Cell viability and metabolic activity in the NP and AF.

(A) The number of live and dead cells across the entire NP area. (B) Representative live/dead staining (green: live cell nuclei, red: dead cell nuclei) from the edge and center of the NP. Scale = 100 μm. (C) The number of live and dead cells in only the central region of the NP. (D) Metabolic activity of cells in the AF region (as measured by the MTT assay). (E) Representative DAPI staining of the AF region to visualize cell distribution within the AF layers (Blue = cell nuclei). Scale = 100 μm. Bars denote significance between groups. * = $p < 0.05$ compared to medium DAPS at the corresponding time point, # = $p<0.05$ compared to all groups.

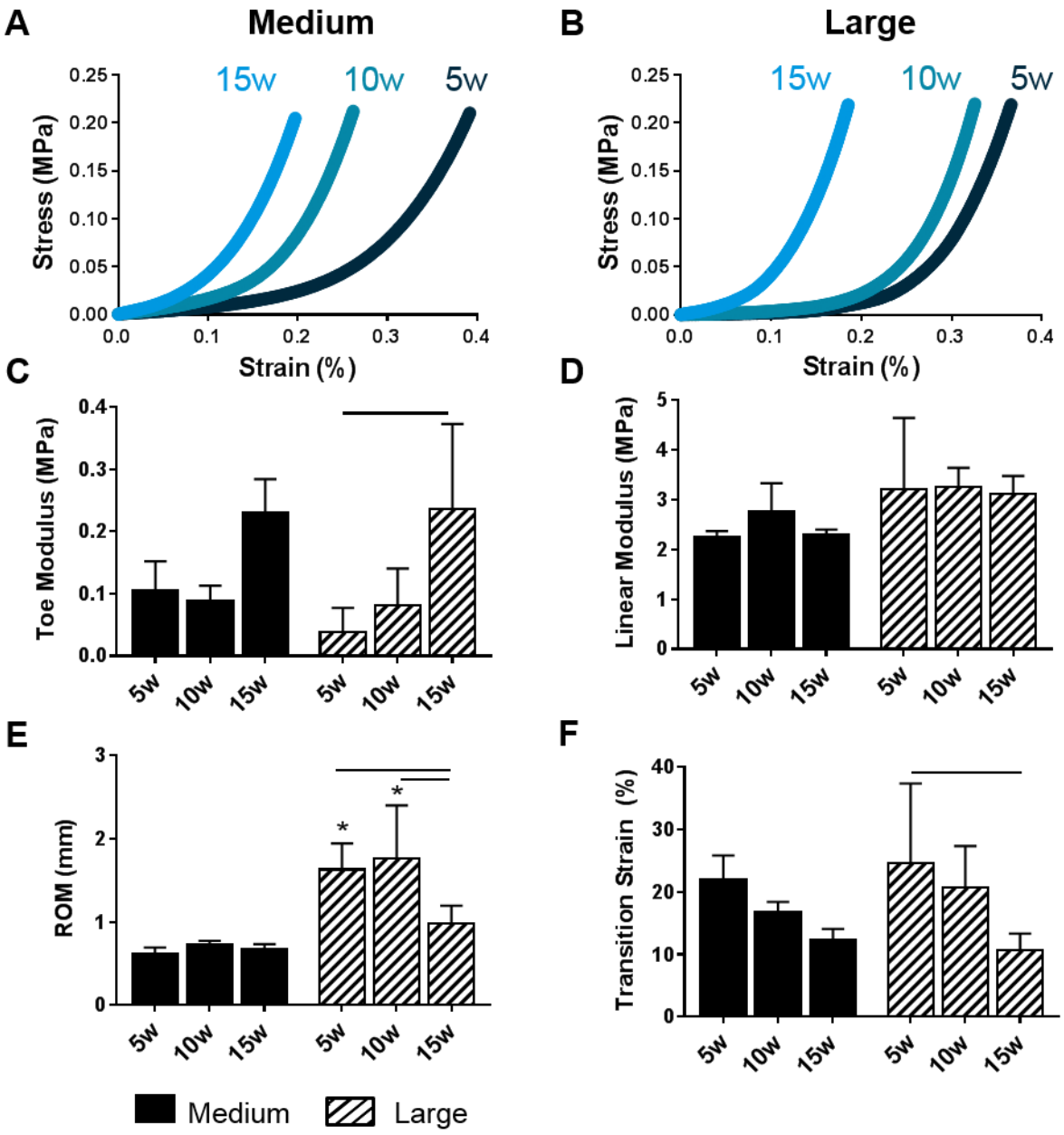

Figure 3. DAPS compressive mechanical properties.

Representative stress-strain curves of (A) medium and (B) large DAPS over the 15 week culture duration. A bi-linear fit was utilized to quantify (C) toe modulus, (D) linear modulus, (E) range of motion, and (F) transition strain. Bars denote significance between groups. * = $p < 0.05$ compared to medium DAPS at the corresponding time point.

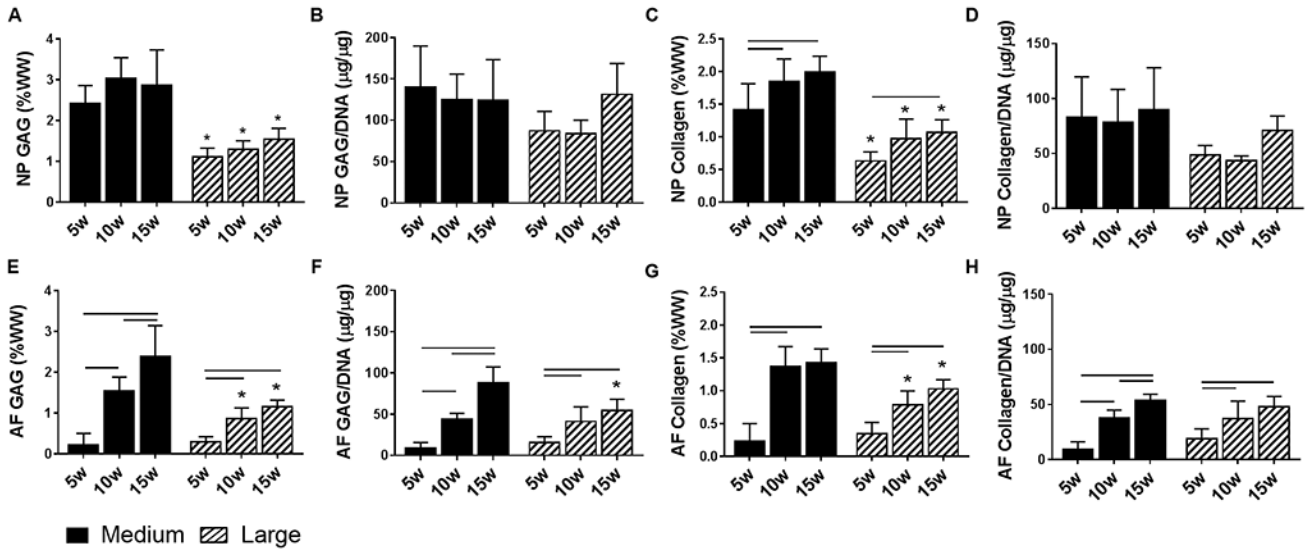

Figure 4. DAPS Biochemical content.

NP GAG content normalized to (A) wet weight and (B) DNA content, and collagen content normalized to (C) wet weight and (D) DNA content as a function of DAPS size and culture duration. AF GAG content normalized to (E) wet weight and (F) DNA content and collagen content normalized to (G) wet weight and (H) DNA content as a function of DAPS size and culture duration. Bars denote significance between groups. * = $p<0.05$ compared to medium DAPS at the corresponding time point.

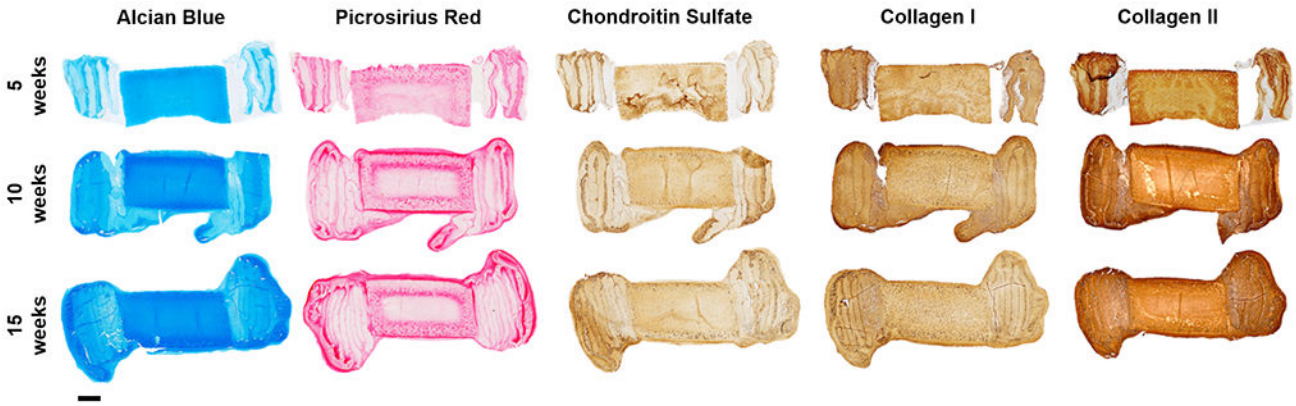

Figure 5. Histologic appearance of medium DAPS.

Representative sagittal sections of medium DAPS at 5, 10, and 15 weeks of culture stained with Alcian blue (glycosaminoglycans) and Picrosirius red (collagens), and immunohistochemical staining for chondroitin sulfate, collagen I, and collagen II. Scale = 1mm.

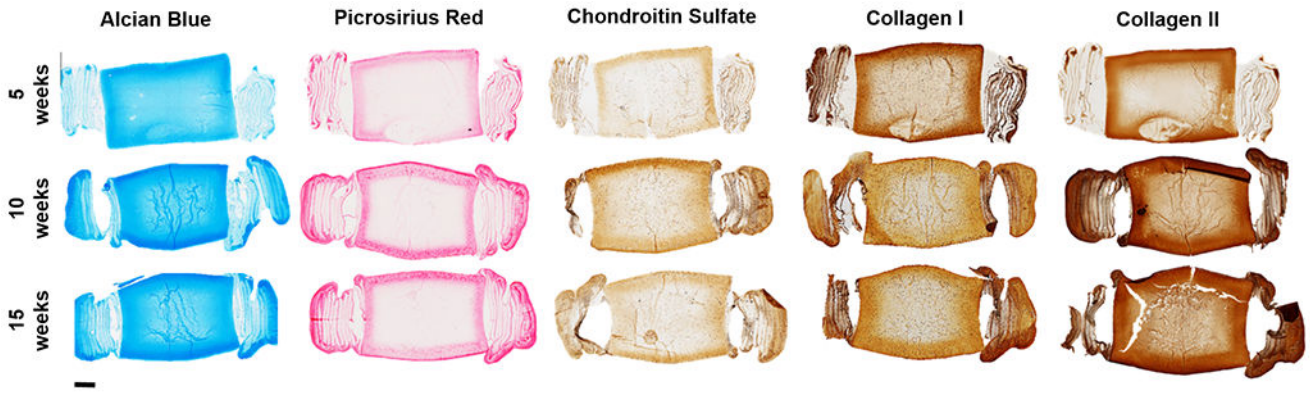

Figure 6. Histologic appearance of large DAPS.

Representative sagittal sections of large DAPS at 5, 10, and 15 weeks of culture stained with Alcian blue (glycosaminoglycans) and Picrosirius red (collagens), and immunohistochemical staining for chondroitin sulfate, collagen I, and collagen II. Scale = 2mm.

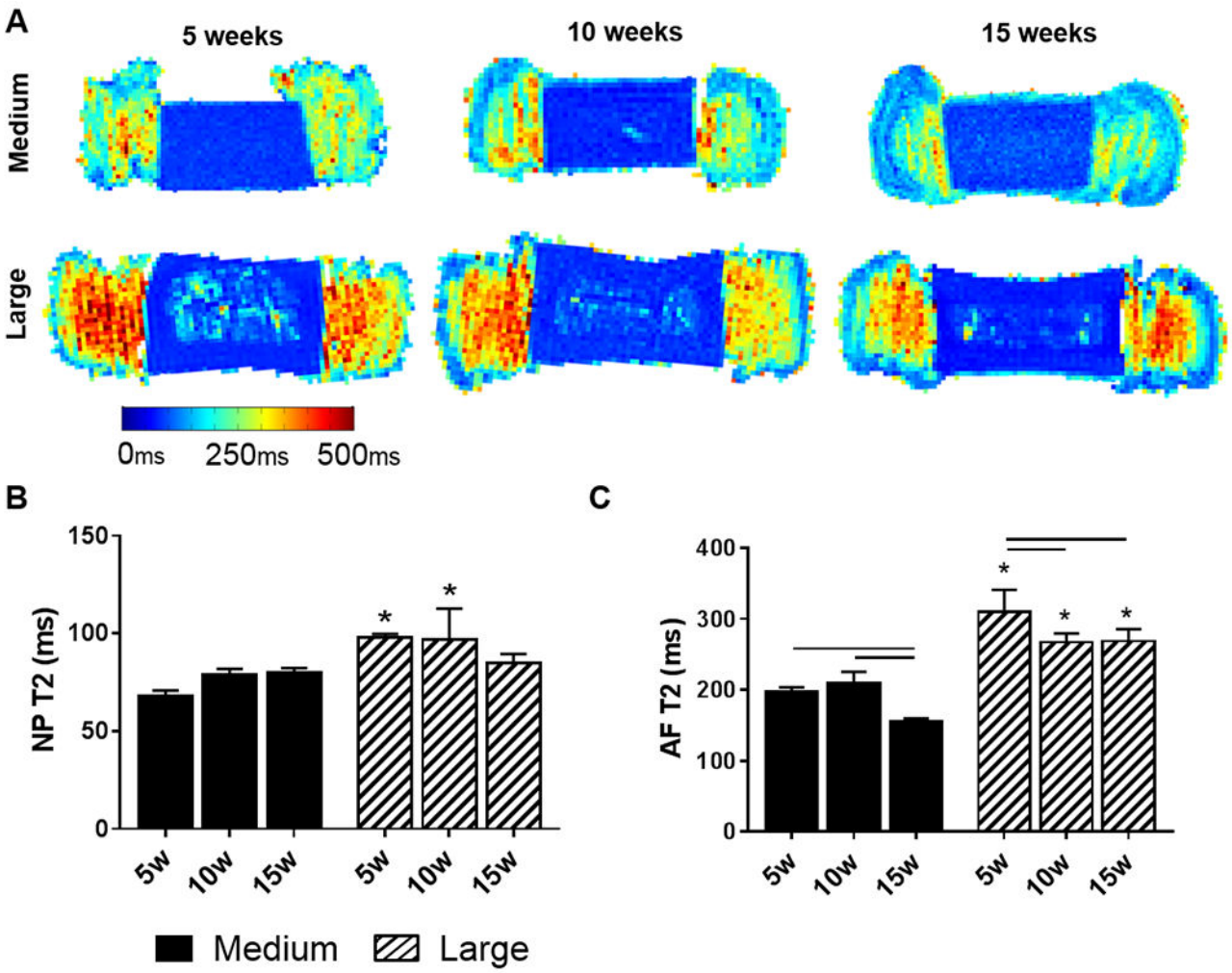

Figure 7. Quantitative MRI T2 mapping of DAPS.

(A) Representative sagittal T2 maps of the medium and large DAPS over the culture duration. The color scale represents the range of T2 values. Quantification of (B) NP and (C) AF T2. Bars denote significance between groups. * = $p<0.05$ compared to medium DAPS at the corresponding time point.

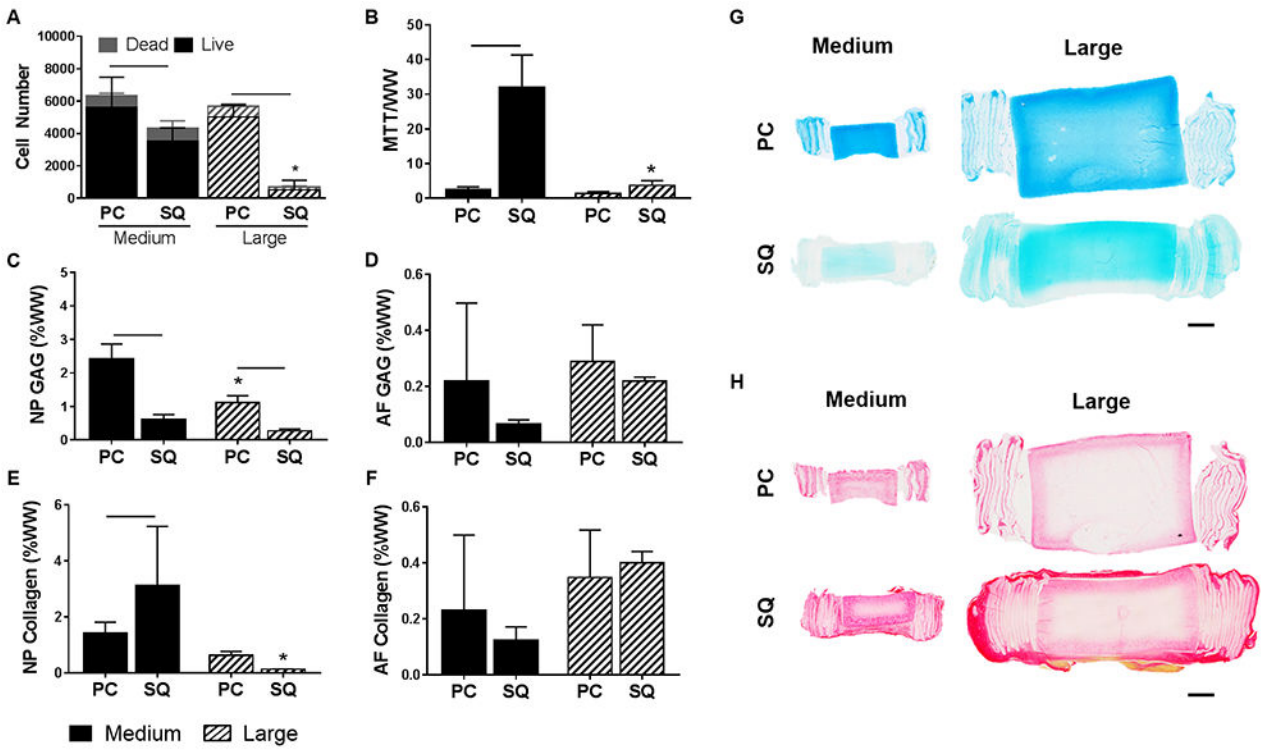

Figure 8. Subcutaneous implantation of DAPS.

(A) Number of live and dead cells across the whole NP area in DAPS pre-cultured for 5 weeks (PC) compared to DAPS implanted subcutaneously (SQ) in athymic rats for 5 weeks after preculture. (B) AF cell metabolic activity as measured by the MTT assay. GAG content in the (C) NP region and (D) AF region normalized to wet weight, and collagen content in the (E) NP region and (F) AF region. Bars denote significance between groups. * = $p<0.05$ compared to medium DAPS at the corresponding time point. Representative (G) Alcian blue and (H) Picrosirius red stained sagittal sections of DAPS after 5 weeks pre-culture and following 5 weeks subcutaneous implantation. Scale = 2 mm.

Table 1.
Comparison of DAPS biochemical content to native discs.

Comparison of the maximal NP and AF GAG and collagen content achieved for medium and large DAPS to that of rabbit, goat and human IVDs.

	Human[28,40]	Large DAPS	Goat[28,40]	Medium DAPS	Rabbit[28,40]
Nucleus Pulposus					
GAG (%ww)	9.3	1.5	5.4	3.0	11.0
Collagen (%ww)	0.3	1.1	2.9	2.0	0.6
Annulus Fibrosus					
GAG (%ww)	2.2	1.2	0.9	2.3	6.0
Collagen (%ww)	3.1	1.0	1.8	1.4	3.0